CSIRO PUBLISHING

International Journal of Wildland Fire **2010**, *19*, 228–237 www.publish.csiro.au/journals/ijwf

Ignition and flame-growth modelling on realistic building and landscape objects in changing environments

Mark A. Dietenberger

USDA Forest Service, Forest Products Laboratory, 1 Gifford Pinchot Drive, Madison, WI 53726, USA.
Email: mdietenberger@fs.fed.us

Abstract. Effective mitigation of external fires on structures can be achieved flexibly, economically, and aesthetically by (1) preventing large-area ignition on structures by avoiding close proximity of burning vegetation; and (2) stopping flame travel from firebrands landing on combustible building objects. Using bench-scale and mid-scale fire tests to obtain flammability properties of common building constructions and landscaping plants, a model is being developed to use fast predictive methods suitable for changing environments imposed on a parcel lot consisting of structures and ornamental plants. Eventually, the property owners and associated professionals will be able to view various fire scenarios with the ability to select building materials and shapes as well as select ornamental plant species and their placement for achieving the desired fire mitigation. The mathematical formulation presented at the 2006 BCC Research Symposium is partially shown here and some results are compared with (1) specialised testing of Class B burning brands (ASTM E108) in the cone calorimeter (ASTM E1354); (2) our refurbished and modified Lateral Ignition and Flame Travel Test (ASTM E1321 and E1317); (3) room-corner tests with oriented-strand board (ISO 9705); and (4) cone calorimeter tests of fire-resistive materials such as fire retardant-treated plywood and single-layer stucco-coated oriented-strand board.

Additional keywords: calorimetry, fire mitigation, flammability modelling.

Introduction

With the increasing fire hazards from wildfires in the United States, homes built in the wildland–urban interface (WUI) will come under increasing regulatory pressures to adopt exterior fire-resistive structures, in addition to managing landscape vegetation and other flammable materials around the building (California code: www.fire.ca.gov/wildland_codes.php and International code: http://www.iccsafe.org/Store/Pages/Product.aspx?category=7710&cat=ICCSafe&id=3850X09, both accessed 3 March 2010). However, it is not always clear as to the effective strategy for wildfire mitigation, even to a fire protection expert. Indeed, homeowners and builders could benefit greatly from a calculation tool for evaluating the wildfire hazards to their structures. Natural fire threats in the WUI basically come in two forms: (1) long-duration exposure from firebrands spotting; and (2) short-duration exposure from heat flux or flame impingement of the wildfire nearing the structure. Threats from adjacent structural fires can be in the forms of long-duration heat flux, flame impingement or firebrands (Babrauskas 2003).

The fire hazard threat of high heat flux or flame impingement from short-duration wildfire exposure is primarily mitigated with vegetative and fuel management in the defence zones around the combustible structures. The kind of vegetative management needed to prevent structural ignition will depend on the fire-resistant construction, the moisture condition of landscape vegetation, and the positions and types of ornamental vegetation relative to the combustible structure (White and Zipperer 2010). To establish the non-threatening distances of rapidly burning ornamental vegetation from a given structure, which may or may not be fire-resistant, one should ideally use a fire-hazard calculation tool, such as the one being partially developed in this paper. The fire-hazard threat of high heat flux or flame impingement from long-duration adjacent structural fires obviously will require greater separation distances between structures, which are typically well understood and part of building regulations (Babrauskas 2003). However, if adjacent structures are fire-resistant, the structure fires on them are likely to be small and of short duration, or non-existent, thereby allowing smaller distances between them. Again, a fire hazard calculation tool would be helpful in revealing this option.

The insidious threat from long-duration firebrand exposure, particularly from those blown in from a distant wildfire, is really the main driving force in requiring fire-resistant structures in the WUI (www.fire.ca.gov/wildland_codes.php, accessed 3 March 2010). Obviously, the owner needs to place wire screens over chimneys, vents, and around decks and windows to prevent firebrand penetration into the highly combustible interiors of buildings (Babrauskas 2003; Manzello *et al*. 2006). However, it is not clear how much fire resistance is needed for the construction exteriors. The homeowner could well decide that the wood deck is expendable as long as the fire (possibly originating in deck crevices with firebrands; Manzello *et al*. 2006) does not spread into the fire-resistant home. Patio doors and windows should also be made resistant to the worst-case firebrand, which is likely similar to the Class A or B simulated firebrand in the ASTM E108 test. The Class A firebrand can also be thought of as multiple firebrands collecting in a corner wall, where the upward flame spread on combustible sidings is likely. The use of an exterior fire

 10.1071/WF07133 1049-8001/10/020228

retardant-treated (FRT) wood siding or similarly fire-resistive material will instead prevent such flame spread, thereby limiting the damage or ignition to the region of direct exposure from the firebrands. Therefore, reasonable and economical design of an exterior fire-resistant construction needs to consider the firebrand threats, even with effective vegetative and fuel management. Indeed, by focussing on reasonable scenarios of firebrands threatening fire-resistant construction exteriors, one can devise a limited prescriptive series of tests that must be met, such as those in the California WUI code, or alternatively provide a fire-hazard calculation tool that can help provide clarity as well as give more options to the homeowner.

For a fire-hazard calculation tool to be realistic for the wildfire threats identified earlier, it must account for variation of flammability properties of common materials, for transient variations of ignition and fire growth on each landscape and structural combustible object, and for the time-changing wildfire exposure from outside the parcel lot. We believe the speed of computer computation has reached the point of bettering the real-time calculation of damage, ignition, and fire growth on combustible objects using specially designed analytical solutions. As Computational Fluid Dynamic codes are far from reaching such a point, we present here certain analytical solutions of the dynamic processes of surface heating to ignition and flame travel that leads to overall fire growth. The key numerical procedure is using stepping boundary conditions to discretise the analytical time integration, which then becomes a fully recursive computation method (Dietenberger 2006*a*). In the next two sections of this paper, the mathematical formulation presented at the 2006 BCC Research Symposium (Dietenberger 2006*b*) is partially shown here for ignition and fire growth. In the additional three sections of this paper, some model results are compared with (1) specialised testing of Class B burning brands (ASTM E108) in the cone calorimeter (ASTM E1354); (2) the refurbished and modified Lateral Ignition and Flame Travel test (LIFT) (ASTM E1321 and E1317); (3) room-corner tests with oriented-strand board (OSB) (ISO9705), and with fire-resistive materials such as FRT plywood and single-layer stucco-coated OSB (see brochure for pictorial descriptions of these tests at website: http://www.fpl.fs.fed.us/research/facilities/fire.shtml, accessed 3 March 2010). These tests were specifically designed or selected to reveal the salient features of wildfire threats to structures, and thereby be suggestive of effective mitigation techniques. We also have available cone-calorimeter and room-corner tests with vegetation (White and Zipperer 2010), but in which fire-growth modelling has yet to be applied.

Ignition predictions with time-changing conditions

The prediction of surface temperature for reaching ignition conditions that take into account the changing boundary conditions, and yet avoid the use of time-consuming finite difference methods as well as avoiding inflexible, approximated, analytical solutions (such as those described in Babrauskas 2003 and Dietenberger 2004), resulted in an innovative mathematical formulation of transient heat transfer. An earlier paper (Dietenberger 2006*a*) published a unique recursive analytical solution for transient heat and moisture transfer in a finitely thick hygroscopic material with time-changing step changes of certain boundary conditions. For many materials, moisture is not a consideration and we show here just the solution for the temperature-change, $T(\hat{x}, t)$, profile due to boundary conditions of time-stepping changes in surface heat fluxes, $\Delta\dot{q}''(\ell, t)$ and back-side heat fluxes, $\Delta\dot{q}''(0, t)$, here as:

$$T(\hat{x}, t) \cong \sum_{i=0}^{n} \left[\frac{\Delta\dot{q}''(\ell, t_i)}{K_{q,\ell}} S(\alpha, \hat{x}, t - t_i) - \frac{\Delta\dot{q}''(0, t_i)}{K_{q,0}} S(\alpha, \ell - \hat{x}, t - t_i) \right] \quad (1)$$

where $\hat{x}$ is dimensional depth, t is current time, ℓ is material thickness, K_q is thermal conductivity coefficient, C_q is heat capacity, ρ is dry body density, $\alpha = K_q/\rho C_q$ is thermal diffusivity, and $S(\alpha, \hat{x}, t)$ is the series expansion solution.

$$S(\alpha, \hat{x}, t) = \frac{\alpha t}{\ell} + \ell \left\{ \frac{3\hat{x}^2 - \ell^2}{6\ell^2} - \frac{2}{\pi^2} \sum_{n=1}^{\infty} \frac{(-1)^n}{n^2} \times \exp\left[\frac{-\alpha t}{1} \left(\frac{n\pi}{\ell} \right)^2 \right] \cos\left(\frac{n\pi\hat{x}}{\ell} \right) \right\} \quad (2)$$

Rarely do classical heat conduction texts discuss such stepping heat fluxes, probably because the summation in Eqn 1 can be burdensome. However, such texts do not offer the possibility of converting Eqn 1 to a recursive summation, as simple and efficient to implement as a computer routine, which we have done for this work. If irradiance, $\dot{q}''_r$, is applied to one surface, the material responds with radiative and convective cooling on the exposed side, and conductive cooling to the thick insulation material on the unexposed side, as in the boundary conditions (see *Nomenclature* section for definitions of abbreviations):

$$\Delta\dot{q}''(\ell, t_i) = \begin{Bmatrix} \alpha_{s,i}\dot{q}''_r(t_i) + \varepsilon_{s,i}\sigma[T_a^4(t_i) - T^4(\ell, t_i)] \\ \quad + h_{c,i}[T_a(t_i) - T(\ell, t_i)] \\ -H(t_i - t_1)\{\alpha_{s,i}\dot{q}''_r(t_{i-1}) + \varepsilon_{s,i}\sigma[T_a^4(t_{i-1}) \\ \quad - T^4(\ell, t_{i-1})] + h_{c,i}[T_a(t_{i-1}) - T(\ell, t_{i-1})]\} \end{Bmatrix}$$

$$\Delta\dot{q}''(0, t_i) = C_{insulate}[T(0, t_i) - T_a(t_i)] - H(t_i - t_1) \times C_{insulate}[T(0, t_{i-1}) - T_a(t_{i-1})] \quad (3)$$

and then eventually the predicted surface temperatures will reach a steady-state value in which the convective and radiative heat losses to the air and conductive heat losses to back-side insulation are equal to radiant energy absorbed. In the case of no back-side insulation, as in the warehouses, the unexposed side will instead have time-changing thermal radiation and convective cooling. The Heaviside function, $H(t_i - t_1)$, is used to specify that before heat exposure, the sample is at a uniform temperature, and therefore has zero heat fluxes at both surfaces. If the irradiance is high enough, then the surface will reach ignition temperature, T_{ig}, before reaching steady-state temperature. To more accurately capture the time at ignition, we used time steps of one second or less, although use of a large time step is feasible if the boundary conditions change slowly enough, as with the diurnal heating cycle.

As can be seen from Eqn 3, the changes in the boundary conditions with time can be used. That is, we can arbitrarily vary

irradiances, convective flow, atmospheric temperature and surface conditions with time. The method can also be extended to multilayered samples in which interfacial zones can be treated as 'conductive back-side cooling' heat transfers. To consider ignition due to flame impingement, we have the imposed heat flux from a 100-kW propane ignition burner (or the firebrand flame or glow), $\dot{q}''_w$, in our room-corner burn tests to use in place of the term $\alpha_s \dot{q}''_r + \varepsilon_s \sigma(T_a^4 - T(\ell,t)^4) + h_{ci}(T_a - T(\ell,t))$ in Eqn 3, as:

$$\dot{q}''_w = \sigma(\alpha_s \varepsilon_f T_f^4 + \varepsilon_s(1-\varepsilon_f)T_a^4 - \varepsilon_s T(\ell,t)^4) + h_{cf}(T_f - T(\ell,t)) \quad (4)$$

The parameters that are known where flux meters have been used in a wall are $\dot{q}''_w = 55\,\mathrm{kW\,m^{-2}}$, $T(\ell,t) = 298\,\mathrm{K}$ and absorptivity and emissivity $\alpha_s = \varepsilon_s = 0.97$. Using averaged measured flame temperature, $T_f = 1173\,\mathrm{K}$, we derived values of the flame emissivity and convective coefficient as $\varepsilon_f = 0.391$ and $h_{cf} = 0.01\,\mathrm{kW\,m^{-2}\,K^{-1}}$ to reproduce the fluxmeter heat flux. Our test materials typically have lower surface emissivity, $\varepsilon_s = 0.88$, and using the above values for other parameters, the imposed heat flux becomes $51\,\mathrm{kW\,m^{-2}}$. Therefore, we would expect the time to ignition on the wall to correlate best with the cone heater flux of $50\,\mathrm{kW\,m^{-2}}$, as was found by Karlsson (1993). However, he used a multiplication factor of 1.7 times the time to ignition from the cone calorimeter to obtain the actual time to ignition for the room-corner test, which is equivalent to adding ~11 s to ignition time due to burner lagging.

Fire growth simulation with changing conditions

In an earlier paper reporting on our ISO9705 tests (Dietenberger and Grexa 1999), we described the complex-variable Laplace transform solution of the Duhamel integral for flame spread, heat-release rate (HRR), and pyrolysis area that involved four stages requiring solution restarts: (1) ignited corner area due to a sluggish propane burner; (2) upward spread of corner flame to the ceiling; (3) lateral spread of top-wall flame for an unlined ceiling; and (4) the pre-flashover rapid downward spreading of the flame on all three combustible walls. This analytical solution was modified for application to the changing conditions of the WUI fire scenario, and the formulation reported in the 2006 BCC Symposium (Dietenberger 2006*b*) is briefly repeated here. The first step in the analysis is the description of the extended flame flux profile as an imposed flux applied over surface distance, y_c, followed by an exponential decay with characteristic length, δ_f, as in:

$$\dot{q}''_{wf}(y) = \dot{q}''_{w0}\left[H(y) + \left(\exp\left\{\frac{-(y-y_c)}{\delta_f}\right\} - 1\right)H(y-y_c)\right] \quad (5)$$

where $H(y)$ is the Heaviside function (see Fig. 1 schematic). With the length of constant flux, y_c, identified with the pyrolysis front, y_p, the characteristic length was found to be proportional to the extended flame length and correlated as $\delta_f = (y_f - y_c)/c_f$, with the value of c_f approximately 1.3 for upward spread. With this spatial profile of flame heat flux, we then analysed for the quasi-steady speed, v_p, of the pyrolysis front by using the formula $y - y_{ig} = v_p(t_{ig} - t)$ in Eqn 5 to represent the sliding movement of the imposed heat flux profile over a given spot until ignition

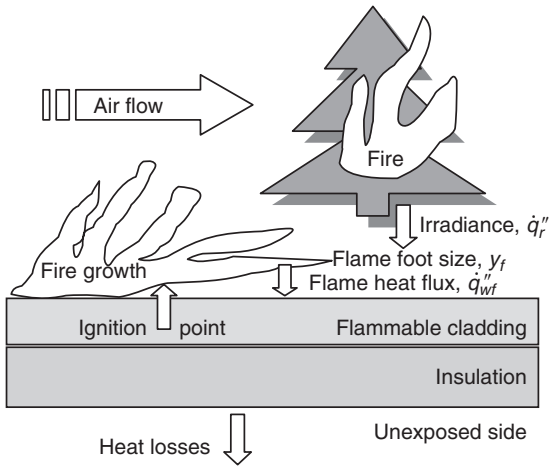

Fig. 1. Schematic of cladding ignition and fire growth.

temperature is reached. With this substitution, Duhamel's superposition integral is the convolution of the material's thermal response to a constant imposed flux with time-changing imposed flux as in:

$$\begin{aligned} T_{ig} - T_m &= \frac{d(T(\ell,t))}{dt} \otimes \dot{q}''_{wf}(v_p(t_{ig} - t) + y_{ig}) \\ &= (T(l,t)) \otimes \frac{d\dot{q}''_{wf}(y_{ig} - v_p(t - t_{ig}))}{dt} \end{aligned} \quad (6)$$

where the integration is taken from zero to the time of ignition, t_{ig}, to correspond to ignition temperature, T_{ig}. We note that Eqn 6 becomes exactly Eqn 1 providing the heat flux profile of Eqn 5 is approximated by incremental flux changes with incremental time steps, which we will show later in evaluating the Lateral Ignition and Flame Travel (LIFT) test data. Because it is possible to have a wide variation in the characteristic flame length, depending on the direction of the flame spread, the time step sizes will have to be highly adaptable to ensure a reasonably accurate and efficient discretisation of Eqn 5 for its use in Eqn 1. If there are multiple flame spread directions on multiple combustible items, then it would be impossible to determine the optimum time steps. This is the fundamental reason why the computational fluid dynamics (CFD) codes, such as the Fire Dynamic Simulator, will fail to predict some types of flame-spreading situations. To avoid this problem, the intricate analytical solution to Eqn 6 (instead of a discretisation solution) for both thermally thick and thermally thin materials and with interpolation between these two regimes is given (Dietenberger 1991) as:

$$\begin{aligned} \delta_f = v_p \tau_m = v_p K_q \rho C_p &\left(\frac{T_{ig} - T_m}{\dot{q}''_{w0} - \dot{q}''_{iq}}\right)^2 \\ &\times \left(\frac{1}{2} + \sqrt{\frac{1}{4} + \left(\frac{K_q(T_{ig} - T_m)}{\ell(\dot{q}''_{w0} - \dot{q}''_{ig})}\right)^{1.3}}\right)^{\left(\frac{-2}{1.3}\right)} \end{aligned} \quad (7)$$

where:

$$\dot{q}''_{ig} = \varepsilon_s \sigma (T_{ig}^4 - T(\ell, 0)^4) + h_c (T_{ig} - T(\ell, 0)) \quad (8)$$

One then realises that all of the material's parameters for thermal response are contained in the material time constant, τ_m, during flame spreading. Closer examination of Eqn 7 shows that the flame travel rate, v_p, can be made quite small with large values for thermal conductivity, material density, heat capacity, material ignition temperature, and material thickness, or with small values for preheated surface temperature, flame heat flux, and flame footprint. Obviously, to completely stop flame spread for any direction, the local flame foot heat flux has been reduced to the critical heat flux needed for ignition (via Eqn 8). The use of fire retardants merely improves on this flame-spread halting, even to the point of diminishing upward flame spread under a strong radiant source. We note that supposed 'constant' fire properties used in Eqns 7 and 8 are also changing with time, especially the flame foot and ignition fluxes.

As the next step in analytical modelling of fire growth, the flame oversize area, $A_f - A_p$, as a non-linear function of HRR (where A_f is flame area on the object and A_p is pyrolysis area on the object), Q_t, and flame width, w, for the corner flame (Dietenberger and Grexa 1999) is linearised at each time step as:

$$2w(y_f - y_p) = 0.0433(2w)^{1/3} Q_t^{2/3} \approx A_{fm} + \frac{\partial A_f}{\partial Q_t}(Q_t - Q_m) + \frac{\partial A_f}{\partial A_p}(A_p - A_{pm}) = c_f(a + bA_p + cQ_t) \quad (9)$$

where A_{fm} is flame area associated with time t_m.

The flame area for other geometries, such as a single vertical wall, a tunnel ceiling, or a circular pool fire, can be similarly linearised for their respective non-linear functions. The fire growth problem, by rearranging Eqn 7, can now be stated concisely as a Voltera-type integral as:

$$\frac{dA_p}{dt} = 2wv_p = \frac{a + bA_p + cQ_t}{\tau_m} + A_{ig,i}\Lambda(t - t_i) \quad (10)$$

where the total HRR is given by a sum of ignition-burner and material-flame-spreading heat release rates as:

$$Q_t = \sum_i \Delta Q_{b,i} H(t - t_i) + \sum_i A_p(t_i) Q''_m(t - t_i) + \int_0^{t-t_i} Q''_m(t - t_i - \xi)\dot{A}_p d\xi \quad (11)$$

where $Q_{b,i}$ is burner heat release rate (kW) associated with time t_i, and

$$Q''_m(t) = Q''_{m,ig} H(t) \exp(-\omega_m t) \quad (12)$$

whereas an exponentially decaying HRR profile (with decay coefficient ω_m) is assumed for a given sample surface, with the peak HRR flux $Q''_{m,ig}$ also changing with time as a result of the changing radiant source. The recursive Laplace solution to Eqn 10 given for each time step is (with the elapsed time after time t_i, $t^* = t - t_i > 0$).

$$A_p(t) = \left(\frac{a + c(Q_{mi} - A_{pi}Q''_{m,iq} + Q_{bi} + \Delta Q_{bi})}{\tau_m} + A_{pi}\omega_m\right) \times \left(\frac{\exp(s_1 t^*) - \exp(s_2 t^*)}{s_1 - s_2}\right) + A_{pi}\left(\frac{s_1 \exp(s_1 t^*) - s_2 \exp(s_2 t^*)}{s_1 - s_2}\right) + \left(\frac{a + c(Q_{bi} + \Delta Q_{bi})}{\tau_m}\right)\left(\frac{\omega_m}{s_1 - s_2}\right) \times \left(\frac{\exp(s_1 t^*) - 1}{s_1} - \frac{\exp(s_2 t^*) - 1}{s_2}\right) \quad (13)$$

$$Q_t(t) = Q_b(t) + Q_m(t) = Q_{bi} + \Delta Q_{bi} + \left(\frac{(a + cQ_{bi})Q''_{m,ig} - b(Q_{mi} - A_{pi}Q''_{m,ig})}{\tau_m}\right) \times \left(\frac{\exp(s_1 t^*) - \exp(s_2 t^*)}{s_1 - s_2}\right) + \frac{cQ''_{m,ig}}{\tau_m}\Delta Q_{bi}\left(\frac{\exp(s_1 t^*) - \exp(s_2 t^*)}{s_1 - s_2}\right) + Q_{mi}\left(\frac{s_1 \exp(s_1 t^*) - s_2 \exp(s_2 t^*)}{s_1 - s_2}\right) \quad (14)$$

where growth acceleration coefficients (in complex variable form) are:

$$s_i = \frac{b + cQ''_{m,ig} - \omega_m \tau_m}{2\tau_m} - (-1)^i \times \sqrt{\left(\frac{b + cQ''_{m,ig} - \omega_m \tau_m}{2\tau_m}\right)^2 + \frac{b\omega_m}{\tau_m}} \quad (15)$$

For brevity, we define the recursive terms, $A_{pi} = A_{ig,i} + A_p(t_i)$, $Q_{bi} = Q_b(t_i)$ and $Q_{mi} = Q''_{m,ig}A_{ig,i} + Q_m(t_i)$. The size of the over-flame area as a function of time is merely given by Eqn 9. As Eqns 13 and 14 are framed in a recursive form, the coefficients and parameters treated as constants during a time step can be allowed to vary from time step to time step. Indeed, the material time constant, τ_m, is in actuality a fairly strong function of time via the changing preheat temperature, T_m, in Eqn 7, which in turn is calculated with Eqn 1 using the time-changing external radiant flux boundary conditions. Therefore, one could conceive that the overall fire growth can switch from a damped fire spread to an accelerative fire spread, or vice versa, through the mere time variation of the material time constant. Because the roots are considered complex numbers, the above solutions are considered to be in the complex variable domain. Specialised computer algorithms were developed for complex evaluations so that the above functions could be programmed directly as a Fortran code called by the Excel spreadsheet. Because of the recursive nature of fire growth equations, it should be possible to consider various changing conditions without recalibrating the coefficients.

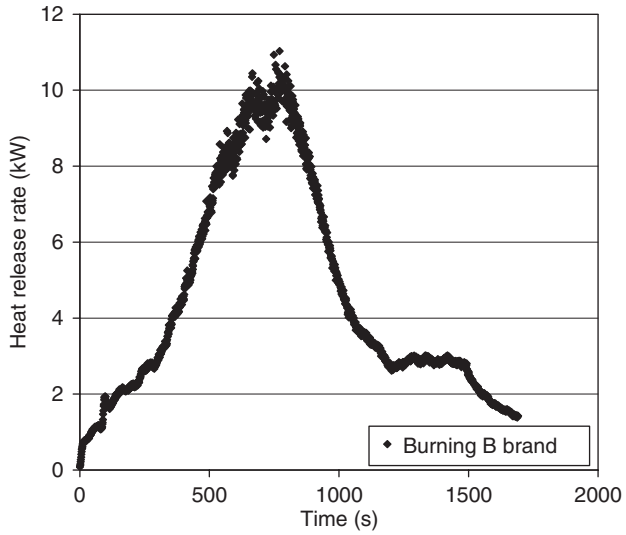

Fig. 2. Heat release rate profile of Class B brand tested in the cone calorimeter.

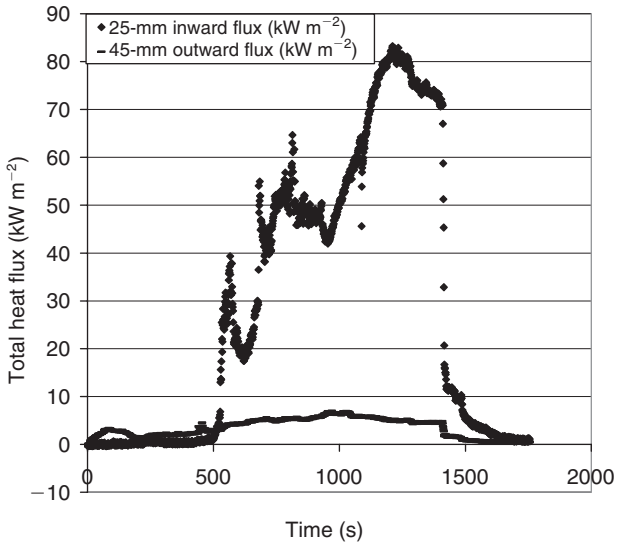

Fig. 3. Measured heat fluxes underneath and outside the burning Class B brand.

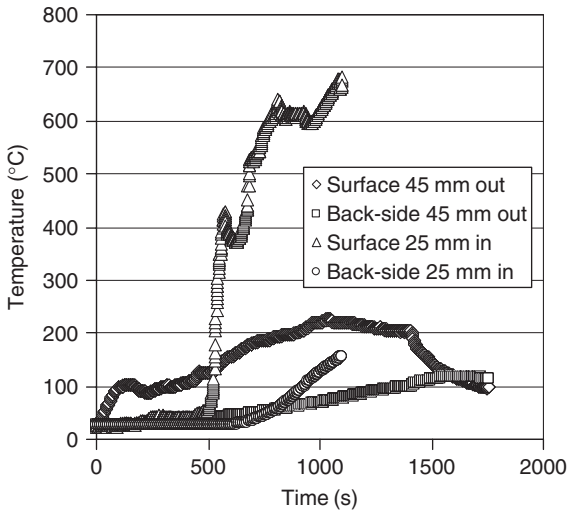

Fig. 4. Analytical prediction of dried redwood response to Class B brand heat exposure.

Class B firebrand tests

To understand the challenges presented in a typical fire scenario in the WUI, we burned the Class B firebrand of ASTM E108 in a cone calorimeter (ASTM E1354) and measured the HRR via the oxygen consumption method. A modified sample-holder was used that allowed air flow into the sample as well as exposed the sample partially to the air. This necessitated turning the cone heater into the vertical position to keep it out of the way, and we opted not to use the cone irradiance, although we may do that in the future. Use of a Bunsen burner to ignite the brand would have been required in the ASTM E108 test to ensure a self-burning brand, but instead, for our test, the brand was partially soaked in a methanol bath. With ignition started at the corners of the brand, the ensuing flame took several minutes to spread around the brand. The measured HRR history as shown in Fig. 2 increases somewhat linearly to a broad peak value of 10 kW and decreases gradually afterwards. Although a simple charring wood surface has a strong initial peak HRR and the HRR then decays approximately exponentially for many seconds, the phenomenon of flame spread around the specimen is rapid enough to result in a net increasing HRR with time. Once flame spreading is finished, the HRR should decay approximately exponentially, but the increasing glowing HRR makes the decrease in the overall HRR less rapid. The fire growth process and the effect on the HRR profile is similarly hypothesised for flaming vegetation, roof fires, deck fires, and so on. The challenge for analytical fire growth modelling is to reproduce the HRR profile with the use of several burning regions in the model.

The heat flux from a burning firebrand, however, varies according to size, distance, shape, view-factor, and time-dependent HRR profile. For example, in our cone calorimeter test of Class B brands, we were able to place one flux meter directly underneath the 150 × 150 × 60-mm wood crib with a 5-mm gap and 25 mm inward from the edge, and another flux meter at 45 mm out from the wood crib. The heat flux data are shown in Fig. 3, which clearly shows the effects of view-factors of the developing flame on the measured value. That is, the outside flux meter seems to mimic the HRR trend and has a peak heat flux of 6.7 kW m^{-2}, which is not enough to ignite most combustible materials but can still char some materials (Babrauskas 2003). However, the flux meter underneath at first could not view the flame, and when the flame came into view, the flux levels eventually reached 50 kW m^{-2}. Then, after the flame subsided and the wood crib was glowing throughout, the flux became as high as 80 kW m^{-2}. This is the high flux that rapidly ignites most combustible materials, and also some fire-resistant materials, albeit with a little more time to ignition (Dietenberger 2004).

Fig. 4 shows the surface temperature response of dried redwood decking, as calculated with Eqn 1 using the imposed heat flux profiles from Fig. 3 as the time-dependent input data. The high temperatures obtained under the 80-kW m^{-2} flux from the

contact with the glowing wood crib confirm the assertion that most combustible building materials will ignite. Yet, a short distance away, the imposed heat flux exposure drops to levels such that most combustible materials will not separately ignite. However, it is possible for flame spread to occur owing to the flame foot heat fluxes, at least until surface cooling fluxes match the sum of imposed radiant flux and flame flux to stop the flame spreading process.

These facts would involve exterior cladding surfaces such as roofs and decks and unprotected interior flooring as highly susceptible to ignition by the 'worse-case' firebrand. Therefore, designing fire-resistant claddings to prevent flame spreading or avoid fire penetrating through the exposed layer after the inevitable ignition would be a desirable trait. Indeed, at least among wood materials, one observes similar ignition behaviour among different species, but their flame spreading behaviour is remarkably different.

Prediction of temperatures during flame spread (LIFT test)

Almost two decades ago, we built the LIFT apparatus (Dietenberger 1994) to duplicate the original at the National Institute of Standards and Technology – Building and Fire Research Laboratory (NIST BFRL), which was developed mainly by Dr Margaret Harkleroad. The intent was to follow the ASTM E1321 standard to obtain ignition and flame spread properties for wood-based materials. The standard called for the 150 × 800-mm (6 × 30-inch) vertically mounted specimen to be exposed continuously to the burner radiant heat until there was a distribution of surface temperature in equilibrium. This distribution of temperature then gave rise to a variation of lateral flame travel rate, which was to be measured manually. However, at the heat fluxes required, the wood was experiencing surface charring, which negated the possibility of deriving flame travel properties. Another factor creating difficulties was the unrealistic high convective flow exposures to cause ignition and flame travel, compared with, for example, the low convective flow involving vitiated hot air in the lateral flame travel phase in the room-corner test (ISO9705). Finally, we were dependent on the Venturi tube to control the burner output with the air flow valve, which created a problem for us when the cyclic central air source caused a highly wandering burner output.

With the current emphasis on WUI applications, installation of a mass-flow controller on the air source, and utilisation of faster and more accurate data acquisition, we embarked on refurbishing the LIFT apparatus. In contrast to the ASTM E1321 standard prescriptions, our modified test protocol involves no surface preheating, numerous tiny surface thermocouples, and a crank-operated computer-recorded indicator for tracking flame position as function of time. The first detailed test involved the OSB boards that were set aside for the LIFT tests after the series of room-corner tests were done in the 1990s. The intent was to use the LIFT tests to derive flame travel properties on OSB that can be used to predict fire growth within the test room lined with the OSB boards.

For the exposure to the 50-kW m^{-2} radiant imposed flux at the 50-mm position from the specimen end, the data (not shown) revealed surface temperature profiles at various locations

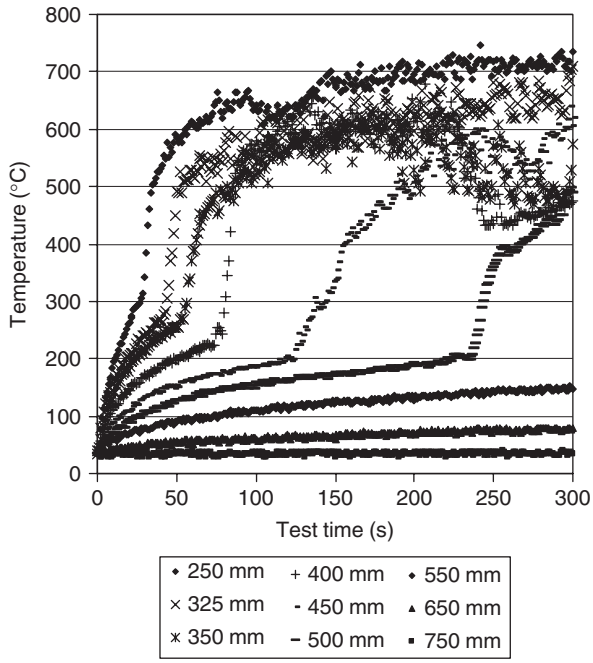

Fig. 5. Surface temperatures measured on oriented-strand board (OSB) surface in the Lateral Ignition and Flame Travel (LIFT) test.

up to 200 mm that are consistent with the flame spread rapidly proceeding downwards from the pilot ignition. In Fig. 5, the surface temperatures profiles at positions greater than 200 mm are shown, in which there was a lateral flame spread that decreased in travel rate until the flame stopped spreading at around 550 mm. Although it is apparent when the flame has travelled over a thermocouple, it was not apparent what the ignition temperature was or just how rapidly the temperature rise had occurred just before the flame-front arrival. Indeed, the rapid rise in temperature after a radiant preheat period indicates that a small flame-foot heating feature must be captured by a credible model of fire growth.

The typical temperature profiles were easily simulated with the recursive formulation of Eqn 1 using reasonable heat flux profiles shown in Figs 6 and 7 with the corresponding temperatures predictions in Figs 8 and 9 compared with the data. The thermophysical properties for OSB were taken from our previous ignitability results (Dietenberger 2004). The imposed heat fluxes required three phases to properly predict surface temperatures. The first phase is the few seconds' increase in heat flux as a result of sliding the specimen into place. At the 50-mm location where the radiant flux was set at ~50 kW m^{-2}, the calculated temperature response reached 301°C at 12 s in Fig. 8. The second phase of heat flux is caused by the flame foot modelled with the time-changing form of Eqn 5, using a flame foot heat flux of 60 kW m^{-2} and a time constant of 0.4 s. The rapid exponential upturn of the temperature was captured using 0.2-s time steps so that the surface temperature of 408°C was obtained at 15.4 s (flame sheet arrival time). Further, but damped, temperature rise resulted from the imposed flux set at 110 kW m^{-2} in this third phase of heating. A similar pattern is noted for Fig. 9, which required a flame foot heat flux of 60 kW m^{-2}, time constant of 4.0 s, and flame sheet arrival time at 83 s. The relative increase

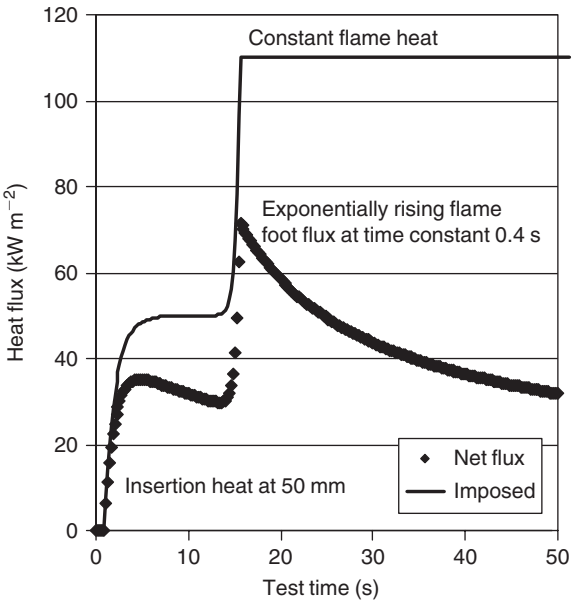

Fig. 6. Imposed heat fluxes modelled for temperature predictions at the 50-mm location.

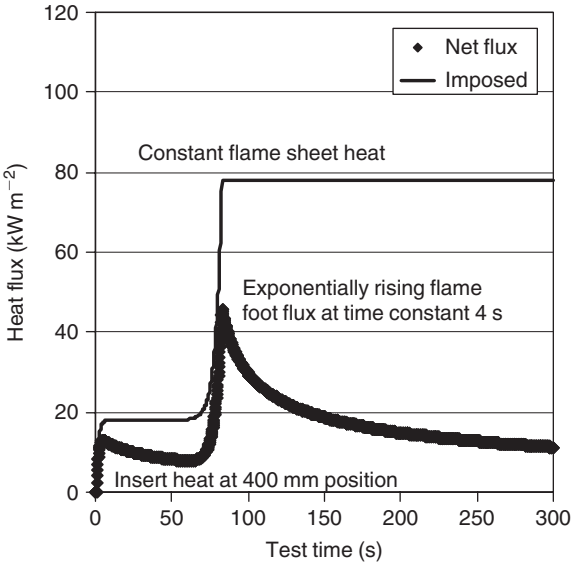

Fig. 7. Imposed heat fluxes modelled for temperature predictions at the 400-mm location.

of the time constant by a factor of 10 meant that the local flame travel rate at 50 mm was also 10 times that at 200 mm. Note that the net surface heat flux due to surface-emitting radiation and reduction in convection heat flux has a rapidly changing profile that is adequately captured by the analytical model to predict the temperature response.

It is interesting that no charring of the wood surface was needed to make close temperature predictions, allowing us to take the planned steps to validate the lateral flame travel rate formula given by Eqn 7. As we have measurements from a

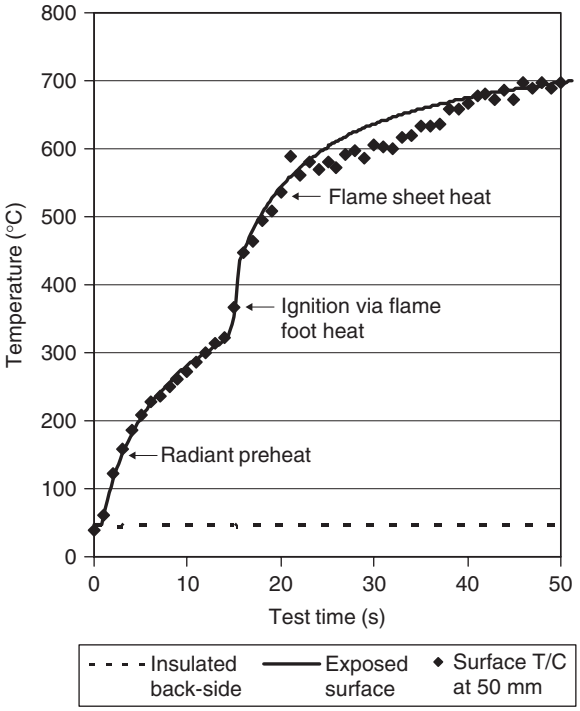

Fig. 8. Prediction of measured surface temperature using imposed heat fluxes in Fig. 5. T/C, thermocouples.

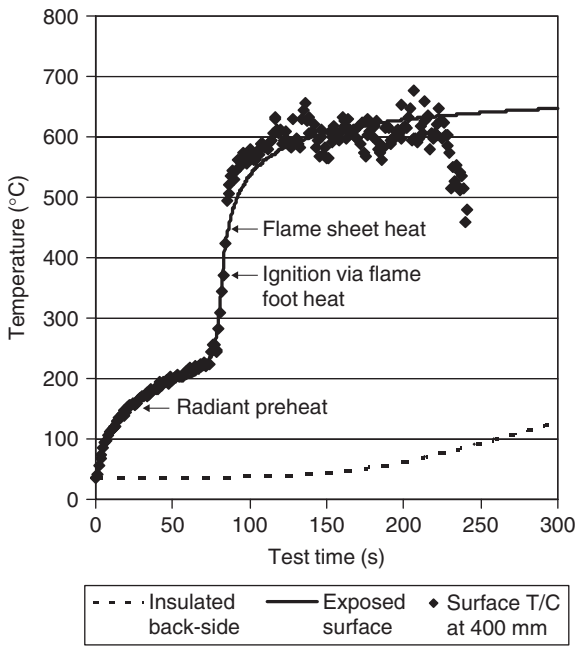

Fig. 9. Prediction of measured surface temperature using imposed heat fluxes in Fig. 6. T/C, thermocouples.

thermopile in the flue gas and from a fume stack thermocouple (ASTM E1317), we can derive the sensible HRR profile (Dietenberger 1994) and compare it with the model-estimated HRR profile from Eqn 14. Success with this approach can be applied to other situations involving flame travel opposing the

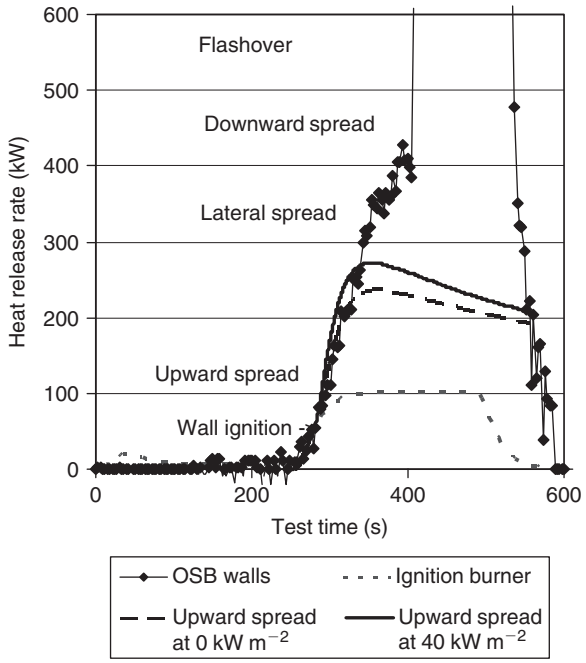

Fig. 10. Analytical prediction and room-corner test for oriented-strand board (OSB) on the walls varying the external radiant flux from 0 to 40 kW m^{-2}.

air flow, such as ground flame propagation or fire on a deck surface.

Selected room-corner tests

Because the analytical fire growth model for changing conditions differs somewhat from the original model, we decided to focus on predicting the upward fire growth behaviour in corner walls, particularly if no approximation of material properties was required and they provided a good representation of the exterior environment (far below flashover conditions). In the case of OSB, we used the properties published earlier (Dietenberger and Grexa 1999; Dietenberger 2004). Fig. 10 shows our room-corner flashover test with OSB linings on the walls and gypsum board on the ceiling. We also show with the dotted smooth curve the ignition burner rising to 100 kW as it is observed by the gas analysers, in which we take into account gas mixing in the test room and gas sensors and time travel of the sampled gas to the sensors. The OSB ignited 25 s after exposure to the ignition burner and led to an upward fire growth that is shown as the HRR profile rising above that of the ignition burner. The dashed smooth curve is predicted by Eqn 14, which was also numerically filtered with a time constant of 18 s for gas lag in the room and a time constant of 10 s for the gas lag in the sensors. The dot-dashed smooth curve is the result of applying an external radiant flux, 40 kW m^{-2}, in addition to that from the ignition burner. This ignited the targeted region at approximately the same time (23.8 s) as the ignition burner. The 'instantaneous' rise in the HRR to a higher peak HRR (which has a delayed peak because of the numerical filters required to simulate gas mixing) demonstrates the capability of the recursive analytical fire growth model to adapt to changing conditions. Several other examples of changing conditions have been applied that showed

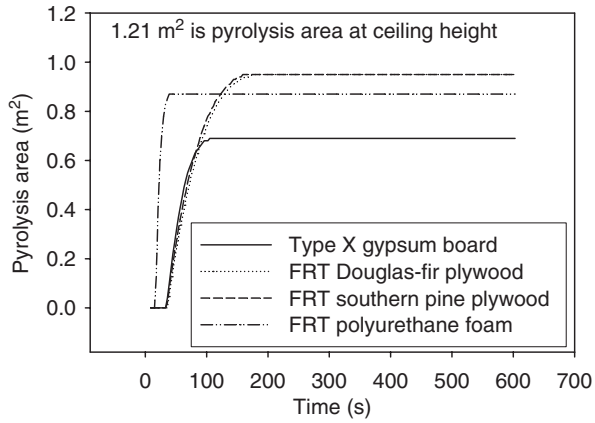

Fig. 11. Prediction of pyrolysis area for upward corner-wall flame spread on FRT (fire retardant-treated) materials subjected to 100-kW burner.

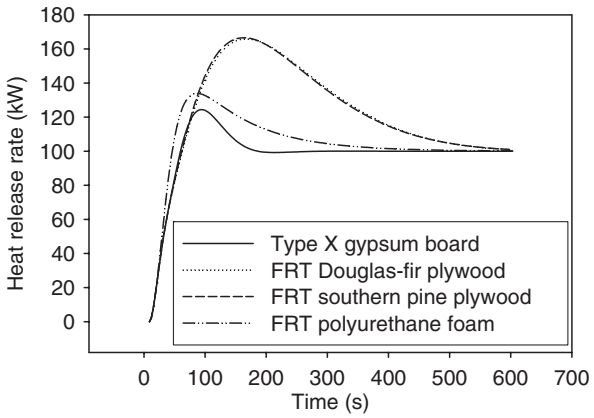

Fig. 12. Prediction of heat-release rate (HRR) for upward corner-wall flame spread on different FRT (fire retardant-treated) materials subjected to 100-kW burner (note: close agreement with room-corner test result was obtained).

reasonable results (not shown). Another type of changing condition we have recently simulated is the effect of fire-resistive linings on reducing and even stopping upward fire growth. Our examples include FRT polyurethane foam, FRT plywoods and Type X gypsum board, shown as burning area plateaus in Fig. 11 and as decaying HRR profiles in Fig. 12, and showing close agreement with associated room-corner tests (Dietenberger and Grexa 1999). Note that the HRR on the Type X gypsum is solely attributed to the combustion of the paper facing. We are not aware of any other analytical fire growth model that has these capabilities of predicting damped fire growth over fire-resistive materials. It is interesting that increasing the ignition burner heat release to 300 kW at 10 min eventually led to room flashovers for all FRT materials except for the Type X gypsum board. Given that we could also cause upward fire growth and flashover for 100-kW ignition-burner flames impinging on the single-layer stucco wall with an OSB substrate, this emphasises the importance of developing the defence zone around the structure to mitigate heat flux or flame impingement threats from wildfire and adjacent structural fire.

Conclusions

The introductory discussions on wildfire threats to constructions and their mitigation have shown the need to understand damage, ignition, and fire growth as exposed to changing conditions on realistic combustible items, including those considered to be fire-resistive. The fire-hazard calculations should ultimately be able to provide (1) the fuel clearance (both vegetation and structure) needed for mitigating large fire threats of high radiant flux or flame impingements on structures; and (2) the mitigation of firebrand threat (from both woodland and housing or structures) to an uninvolved structure with different types of economical fire-resistive claddings. Thus far, we have shown how the use of data from the bench-scale cone calorimeter and from various flame travel tests such as LIFT, the room-corner test and the radiant panel, can be used in analytically based fire-growth models adaptable to changing conditions. At the present level of development, it seems premature to provide a table of parameter values used in the model, but we hope to remedy this soon when the ignition and fire growth model has been further calibrated, tested, and documented. Ultimately, we believe that by providing a fire-hazard tool based on fire-growth algorithms associated with ornamental vegetation and fire-resistive exteriors in changing environments as proposed here, the client will be able to find an optimum and economical fire-safe construction and landscaping.

For various test apparatus mentioned in the present paper see:

- Fire research program brochure: http://www.fpl.fs.fed.us/research/facilities/fire.shtml.
- Publications: www.fpl.fs.fed.us/document-lists/firelist.html.

References

Babrauskas V (2003) 'Ignition Handbook.' (Fire Science Publishers: Issaquah, WA)

Dietenberger MA (1991) Piloted ignition and flame spread on composite solid fuels in extreme environments. PhD dissertation, University of Dayton, OH.

Dietenberger MA (1994) Protocol for ignitability, lateral flame spread, and heat release rate using LIFT apparatus. In 'Fire and Polymers II. Materials and Tests for Hazard Prevention: Proceedings of 208th National Meeting of the American Chemical Society August 1994', 21–26 August 1994, Washington, DC. (Ed. GL Nelson) ACS Symposium Series 599, Chapt. 29. (American Chemical Society: Washington, DC) Available at http://www.fpl.fs.fed.us/documnts/pdf1995/diete95c.pdf [Verified 3 March 2010]

Dietenberger MA (2004) Ignitability of materials in transitional heating regimes. In 'Wood & Fire Safety: Proceedings, 5th International Scientific Conference', 18–22 April 2004, Svolen, Slovakia. pp. 31–41. (Faculty of Wood Sciences and Technology, Technical University of Zvolen: Zvolen, Slovakia) Available at http://www.fpl.fs.fed.us/documnts/pdf2004/fpl_2004_dietenberger001.pdf [Verified 22 March 2010]

Dietenberger MA (2006*a*) Using a quasi-heat-pulse method to determine heat and moisture transfer properties for porous orthotropic wood products or cellular solid materials. *Journal of Thermal Analysis and Calorimetry* **83**(1), 97–106. doi:10.1007/S10973-005-7068-Y

Dietenberger MA (2006*b*) Analytical modeling of fire growth on fire-resistive wood-based materials with changing conditions. In 'Proceedings of the Conference on Recent Advances in Flame Retardancy of Polymeric Materials, Volume XVII: Applications, Research and Industrial Development Markets', August 2006, Norwalk, CT. pp. 13–24. (BCC Research: Nowalk, CT) Available at http://www.fpl.fs.fed.us/documnts/pdf2006/fpl_2006_dietenberger002.pdf [Verified 3 March 2010]

Dietenberger MA, Grexa O (1999) Analytical model of flame spread in full-scale room/corner tests (ISO9705). In 'Fire and Materials 1999 6th International Conference' 22–23 February 1999, San Antonio, TX. (Eds M Janssens, S Grayson) (Interscience Communications Ltd: London) Available at http://www.fpl.fs.fed.us/documnts/pdf1999/diete99a.pdf [Verified 3 March 2010]

Karlsson B (1993) A mathematical model for calculating heat release rate in the room-corner test. *Fire Safety Journal* **20**, 93–113. doi:10.1016/0379-7112(93)90032-L

Manzello SL, Cleary TG, Shields JR, Yang JC (2006) On the ignition of fuel beds by firebrands. *Fire and Materials* **30**, 77–87. doi:10.1002/FAM.901

White RH, Zipperer WC (2010) Testing and classification of individual plants for fire behaviour: plant selection for the wildland–urban interface. *International Journal of Wildland Fire* **19**, 213–227. doi:10.1071/WF07128

Manuscript received 2 August 2007, accepted 22 May 2009

Nomenclature

$\alpha_s = \varepsilon_s$, surface absorptivity equal to surface emissivity for most building materials
δ_f, exponential decay with characteristic length for flame extension (m)
ε_f, flame emissivity
ω_m, decay coefficient for material burn-off ($1\ s^{-1}$)
ρ, dry body density ($kg\ m^{-3}$)
$\alpha = K_q/\rho C_q$, thermal diffusivity ($m^2\ s^{-1}$)
σ, Stefan–Boltzmann constant ($kW\ K^{-4}\ m^{-2}$)
τ_m, material time constant (s)
A_f, flame area on combustible object (m^2)
A_p, combustible object pyrolysis area (m^2)
C_q, heat capacity ($kJ\ kg^{-1}\ K^{-1}$)
$H(t_i - t_1)$, Heaviside function
h_{cf}, flaming convective coefficient ($kW\ m^{-1}\ K^{-1}$)
Q_t, HRR, total heat release rate (kW)
$Q''_{m,ig}$, material peak HRR flux ($kW\ m^{-2}$)
K_q, thermal conductivity coefficient ($kW\ m^{-1}\ K^{-1}$)
ℓ, material thickness (m)
$\Delta\dot{q}''(\ell, t)$, time stepping changes in surface heat fluxes ($kW\ m^{-2}$)
$\Delta\dot{q}''(0, t)$, time stepping changes in back-side heat fluxes ($kW\ m^{-2}$)
$\dot{q}''_r$, irradiance ($kW\ m^{-2}$)
$\dot{q}''_w$, imposed heat flux from ignition burner or the firebrand flame and glow ($kW\ m^{-2}$)
s_i, growth acceleration coefficients (Eqn 15)
$S(\alpha, \hat{x}, t)$, series expansion solution (Eqn 2)
t, current time (s)
$T(\hat{x}, t)$, temperature change (K)
T_f, averaged measured flame temperature (K)
T_{ig}, ignition temperature (K)
v_p, quasi-steady speed of surface flame spread ($m\ s^{-1}$)
w, flame width (m)
$\hat{x}$, dimensional depth (m)
y, surface distance (m)